

studying the dynamics of many-body systems and quantum distillation of states (31).

Recently, we theoretically investigated how quantum information interacts with quantum many-body physics (32), wherein the many-body entanglement structures (33, 34) played an essential role in characterizing different quantum phases.

Conclusion

We expect that more researchers will join the quantum information and computation groups of IOP. In fact, several national programs have been organized to promote the research of quantum information processing. IOP will be a crucial part of these projects. In addition, we plan to play a more important role both in China and worldwide in developing quantum computation and quantum information processing for industrial and scientific applications.

References

1. S. P. Zhao *et al.*, *Phys. Rev. B* **72**, 184511 (2005).
2. X. B. Zhu *et al.*, *Phys. Rev. B* **73**, 224501 (2006).
3. S. X. Li *et al.*, *Phys. Rev. Lett.* **99**, 037002 (2007).
4. H. F. Yu *et al.*, *New J. Phys.* **15**, 095006 (2013).
5. H. F. Yu *et al.*, *Phys. Rev. B* **81**, 144518 (2010).
6. H. F. Yu *et al.*, *Phys. Rev. Lett.* **107**, 067004 (2011).
7. G. M. Xue *et al.*, *Phys. Rev. B* **90**, 224505 (2014).
8. Y. Tian *et al.*, *Rev. Sci. Instrum.* **83**, 033907 (2012).
9. H. K. Xu *et al.*, *Nat. Commun.* **7**, 11018 (2016).
10. W. Yu-Lin *et al.*, *Chin. Phys. B* **22**, 090312 (2013).
11. H. Deng *et al.*, *IEEE Trans. Appl. Supercond.* **25**, 1–4 (2015).
12. Y. L. Wu *et al.*, arXiv:1605.06747 (2016).
13. Y. R. Zheng *et al.*, *Phys. Rev. Lett.* **118**, 210504 (2017).
14. C. Song *et al.*, *Nat. Commun.* **8**, 1061 (2017).
15. C. Song *et al.*, *Phys. Rev. Lett.* **119**, 180511 (2017).
16. K. Xu *et al.*, *Phys. Rev. Lett.* **120**, 050507 (2018).
17. C. Nayak *et al.*, *Rev. Mod. Phys.* **80**, 1083–1159 (2008).
18. V. Mourik *et al.*, *Science* **336**, 1003–1007 (2012).
19. S. Nadj-Perge *et al.*, *Science* **346**, 602–607 (2014).
20. F. Yang *et al.*, *Phys. Rev. B* **85**, 104508 (2012).
21. Y.-Y. Zhu *et al.*, *Chin. Phys. Lett.* **34**, 067301 (2017).
22. L. Fu, C. L. Kane, *Phys. Rev. Lett.* **100**, 096407 (2008).
23. F. Qu *et al.*, *Sci. Rep.* **2**, 339 (2012).
24. Cao, T. *et al.*, *Nat. Commun.* **3**, 887 (2012).
25. Wang, G. *et al.*, *Phys. Rev. Lett.* **117**, 187401 (2016).
26. G. Q. Liu *et al.*, *Nat. Commun.* **4**, 2254 (2013).
27. G. Q. Liu *et al.*, *Nat. Commun.* **6**, 6726 (2015).
28. Z. Feng *et al.*, *Chin. Phys. Lett.* **32**, 123701 (2015).
29. X. Y. Luo *et al.*, *Sci. Rep.* **6**, 18983 (2016).
30. J. Q. Fu *et al.*, *Chin. Phys. B* **25**, 010302 (2016).
31. L. Xia *et al.*, *Nat. Phys.* **11**, 316–320 (2015).
32. B. Zeng, X. Chen, D. L. Zhou, X. G. Wen, arXiv:1508.02595 (2015).
33. D. L. Zhou, *Phys. Rev. Lett.* **101**, 180505 (2008).
34. J. Cui *et al.*, *Nat. Commun.* **3**, 812 (2012).

Light–matter interactions

Ling Lu*, Rongjuan Liu,
Xiulai Xu, Chen Ge, Kuijuan Jin,
Li Wang, and Guozhen Yang

Here, we highlight a few directions of research being pursued at the Key Laboratory of Optical Physics, on light–matter interactions between microwave, terahertz, and subwavelength structures as well as optical photons, quantum emitters, oxide films, and biological samples.

Topological photonics

Topology, a branch of mathematics that recently found wide applications in science, is concerned with the invariant properties of an object undergoing continuous transformation. Consequently, any physical quantity expressed by discrete topological invariants is unprecedentedly robust against large perturbations. The 2016 Nobel Prize in physics was awarded for research on topological physics. Likewise, photonics is also benefiting from band topologies—discrete global configurations of wave-functions in the Brillouin zone of periodic systems such as photonic crystals. Using topological photonics, photon transport without any localization and scattering loss is now feasible.

Since the concept of photonic crystals was first proposed in 1987, Group L01 has been working on experiments with periodic dielectric materials. In 1994, our group reported laser-assisted crystallization of polystyrene spheres and strontium titanate (SrTiO₃) particles ($n = 2.5$) with lattice constants of $\sim 1.5 \mu\text{m}$ (1). Such photonic crystals are characterized by their band structures, while the hidden freedom of band topology was only unveiled in 2005. Topological photonics started with the proposal of a one-way waveguide as the edge state of a two-dimensional (2D) photonic crystal, which was experimentally demonstrated in 2009. In the following year, our group published the second set of experimental results (2) on this topic in the context of microwave frequencies. The idea is illustrated in Figure 1A. The edge mode of a magnetic photonic crystal has a gapless dispersion curve traversing the whole bandgap, connecting the bulk bands above and below. The group velocity of the edge mode has only one sign and propagates in one direction only, without scattering from arbitrary defects. Such a one-way edge state is analogous to the chiral edge state in the quantum Hall effect, providing a novel mechanism for planar integration of nonreciprocal photonic devices.

In three dimensions, optical fibers are the best light guides and are ubiquitous in modern technologies. Using high-dimensional band topologies, we have shown that one-way fibers can be designed using 3D magnetic photonic crystals (3), as illustrated in Figure 1B. These

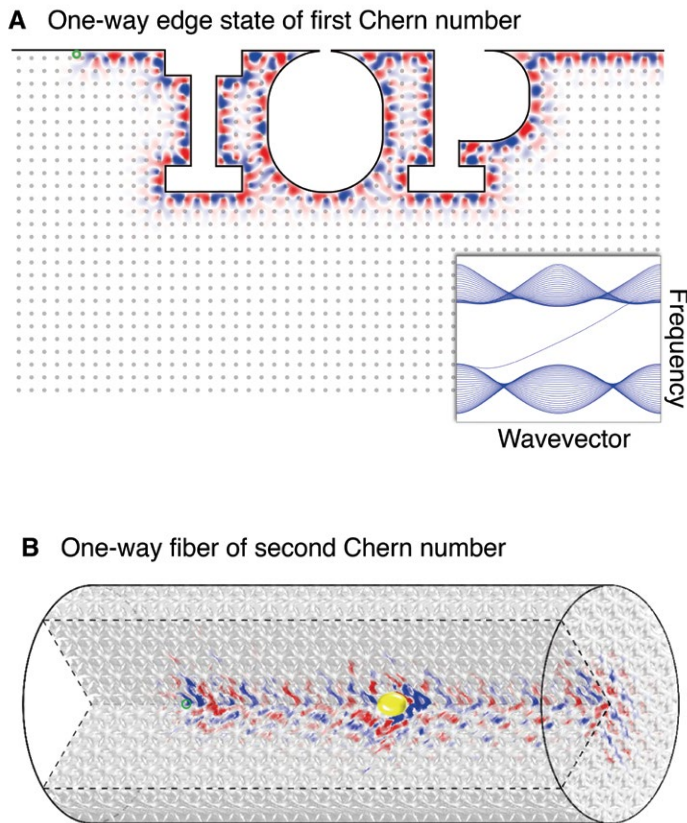


FIGURE 1. Topological one-way waveguides in two and three dimensions. (A) Simulation of a one-way edge state, in a two-dimensional magnetic photonic crystal, immune to backscattering from arbitrary defects. The band structure is plotted as the inset. (B) Simulation of wave propagation around a metallic sphere inside a one-way fiber, designed using a topological line defect in a three-dimensional magnetic photonic crystal. The green circles indicate continuous-wave point sources.

one-way fiber modes were realized by introducing a topological line defect within a fully gapped topological photonic crystal. Unlike the one-way edge states protected by the first Chern numbers defined in the 2D Brillouin zone, our one-way fiber modes are protected by the second Chern numbers defined in the four-dimensional (4D) parameter space, including the 3D momentum space and the winding angle associated with the helical line defects.

The above one-way edge states and fiber modes are only two intuitive examples of the potential of topological photonics (4). Topological band structures in three dimensions remain largely unexplored. For example, nodal lines can have nontrivial connectivity, such as the nodal chains that we demonstrated experimentally (5). Useful device designs and applications are anticipated in many areas of photonics using topology.

Solid-state quantum optics

Solid-state quantum optics has encouraged pronounced advances in the implementation of quantum information processing. Group L02 focuses primarily on the quantum-state control of single quantum dots (QDs), QD-cavity coupling for cavity quantum electrodynamics (CQED), and scaling up for quantum photonic networks. Self-assembled QDs, such as InAs/GaAs QDs, are 3D-confined nanostructures grown by molecular-beam epitaxy. Owing to quantum confinement, the QDs have atom-like discrete energy levels and are key elements for solid-state quantum optics.

The spins of electrons and holes in a single QD have long coherence time at low temperatures, which makes QDs one of the best candidates for quantum bits (qubits). With a single QD embedded in the intrinsic region of a Schottky photodiode, the charge states in the QD can be controlled precisely by applying DC electric and magnetic fields. For example, we demonstrated that the dipole moment of an exciton in a QD can be inverted, when the carrier wave functions shrink with the applied magnetic field (6). In addition, the diamagnetic energy shifts of excitons can be greatly enhanced when the carrier wave functions extend into the underlying wetting layer. Figure 2A shows the magneto-photoluminescence of a single QD. With a bias voltage of 0.5 V, additional weak emission lines appear to have much larger energy shifts, compared with the normal exciton emissions (X^+ , XX^+ , and X^{2+}) labeled in the left panel. This may offer a novel platform to control the interactions between QDs and the surrounding environment (7).

An advantage of semiconductor QDs is their monolithic integration with optical cavities as a CQED system. One potential application of CQED is nonclassical photon sources. As shown in Figure 2B, we proposed a two-beam scheme to implement a strong photon blockade with a single QD in a nanocavity (8). By driving the cavity and the QD simultaneously by two laser fields

with frequency ω_L and ω_p of specific phases, the photon blockade can be substantially enhanced because of the destructive quantum interference of the two-photon excitation in the cavity. In this scenario, the calculated second-order correlation function $g^{(2)}(0)$ is lower by over two orders of magnitude than the traditional values.

Experimentally, the Purcell enhancement of colloidal QDs in a microdisk was demonstrated at room temperature in the weak coupling regime (9). To achieve strongly coupled exciton-polariton states, we designed and fabricated the L3 photonic crystal cavity embedded with a single QD. Figure 2C shows a scanning electron microscopy image of the cavity as well as the corresponding optical modal profile. The measured quality factor of the cavity is around 11,000, as shown in Figure 2D. As illustrated in Figure 2E, an integrated device with coupled photonic crystal cavities and waveguides has been designed to implement ultrafast

FIGURE 2. Physical mechanism and devices of quantum dots (QDs). (A) Photoluminescence spectra as a function of magnetic fields and different bias voltages. Much larger energy shifts of the excitons were observed with weaker emission intensities compared to the regular excitons labeled as X^- , XX^- , and X^{2-} , known as the negatively charged exciton, negatively charged bi-exciton, and double negatively charged exciton, respectively. (B) A new scheme for photon blockade. The cavity and the QD are driven simultaneously by two laser fields with frequency ω_L and ω_p . A transmission electron microscope image of the QD is shown as the inset. (C) A scanning electron microscope image and calculated mode profile of the L3 photonic crystal cavity embedded with QDs. (D) Cavity quality factor or Q factor=11,000. (E) An integrated device with coupled nanocavities and waveguides to implement ultrafast laser switching for a solid state-based photonic network.

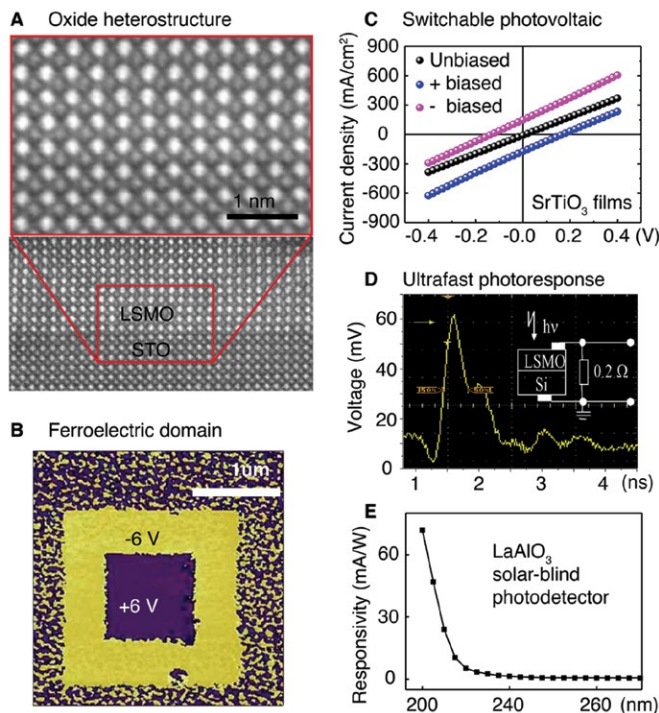
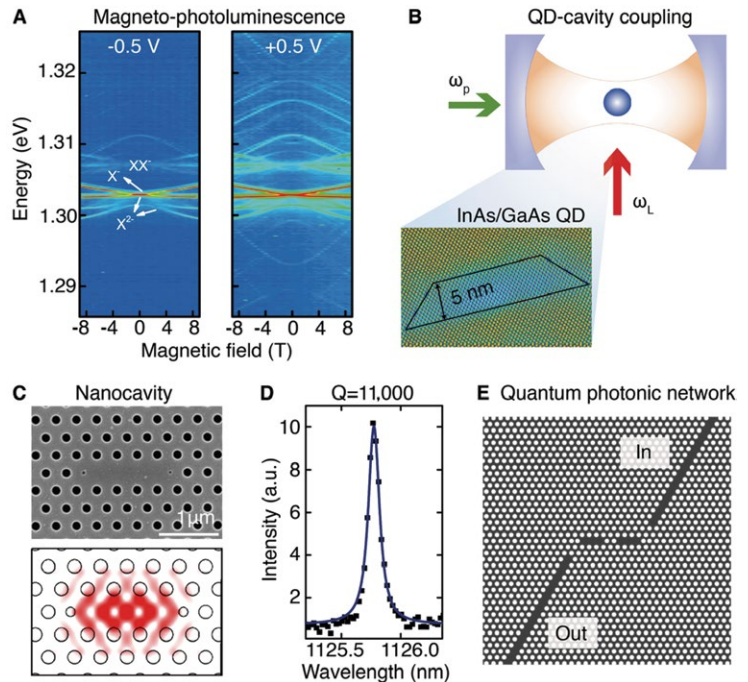


FIGURE 3. Multifunctional perovskite-oxide films. (A) Transmission-electron-microscopy image of lanthanum strontium manganite/strontium titanate ($\text{La}_{0.8}\text{Sr}_{0.2}\text{MnO}_3/\text{SrTiO}_3$) interface. (B) Out-of-plane piezoresponse force microscopy phase map of an 8-nm bismuth ferrite (BiFeO_3) film. (C) Photocurrents of the pristine, positively and negatively biased strontium titanate photovoltaic devices based on SrTiO_3 films under the illumination of a 375-nm laser. (D) Ultrafast photoresponse of an $\text{La}_{0.7}\text{Sr}_{0.3}\text{MnO}_3/\text{silicon}$ (Si) heterojunction. (E) Spectral response of the lanthanum aluminum oxide (LaAlO_3) photodetector under a 10-V bias. LSMO, lanthanum strontium manganite; STO, strontium titanate.

optical switching with a time scale of a few picoseconds due to energy oscillation between the two cavities (10).

Perovskite-oxide optoelectronics

The well-known perovskite structure, ABX_3 , is a rich platform in materials science. For example, solution-based perovskite solar cells with an organic A-site and halide

X-site were recently reported to have substantial increase in efficiencies (>20%). In the past few decades, epitaxial perovskite oxide (ABO_3) films and heterostructures have attracted considerable attention for their physical properties as well as their potential device applications. Laser molecular beam epitaxy (LMBE) is one of the most popular methods to deposit high-quality perovskite oxide

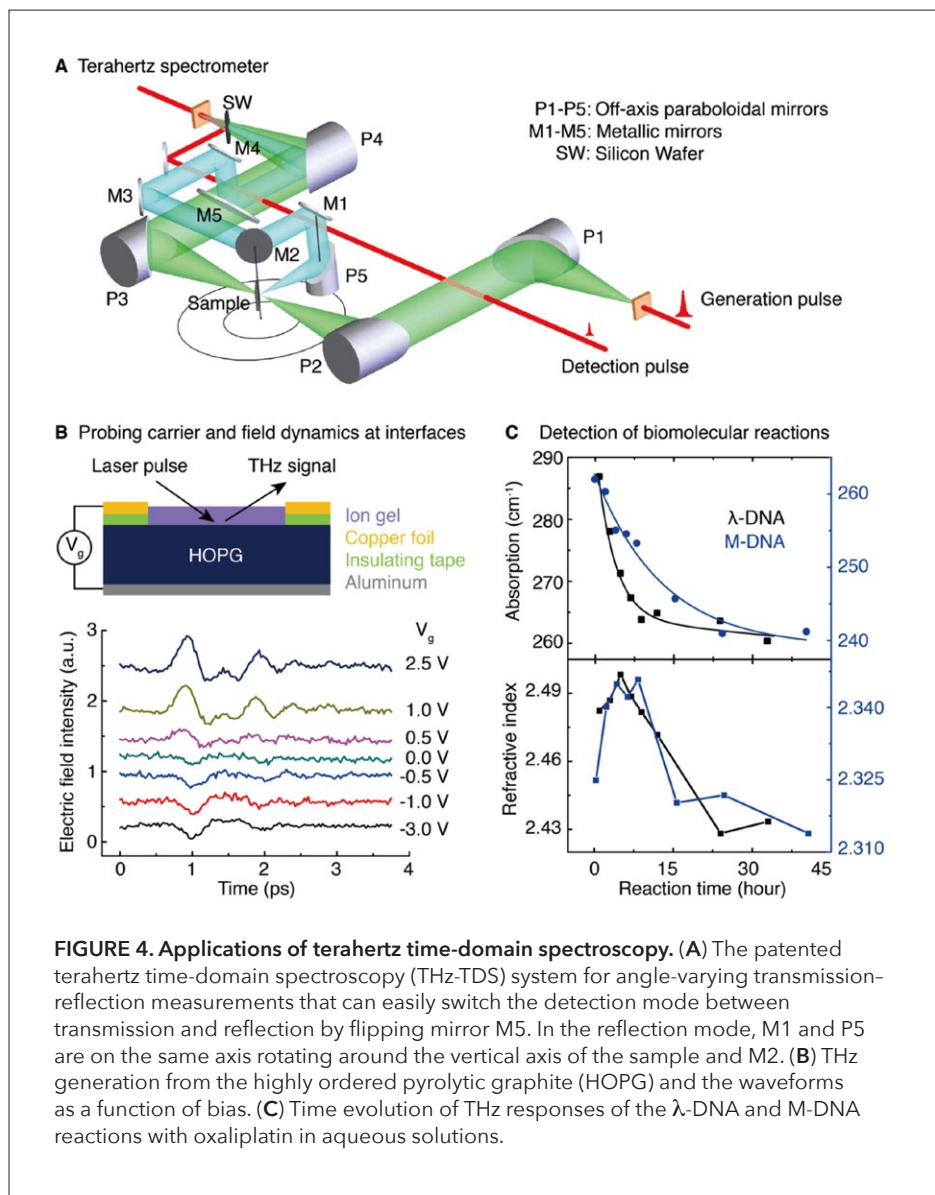


FIGURE 4. Applications of terahertz time-domain spectroscopy. (A) The patented terahertz time-domain spectroscopy (THz-TDS) system for angle-varying transmission-reflection measurements that can easily switch the detection mode between transmission and reflection by flipping mirror M5. In the reflection mode, M1 and P5 are on the same axis rotating around the vertical axis of the sample and M2. (B) THz generation from the highly ordered pyrolytic graphite (HOPG) and the waveforms as a function of bias. (C) Time evolution of THz responses of the λ -DNA and M-DNA reactions with oxaliplatin in aqueous solutions.

films due to its outstanding performance and ease of use. Briefly, the deposition of perovskite oxide film via LMBE is achieved by vaporization of target materials using a pulsed laser in a reactive environment.

Group L03 designed China's first LMBE equipment about three decades ago, and has successfully demonstrated many functional films such as ferromagnetic, ferroelectric, and optoelectronic perovskite-oxide heterostructures with atomically sharp interfaces (Figure 3A) (11, 12). For instance, the lanthanum strontium manganite/strontium niobium titanate ($\text{La}_{0.9}\text{Sr}_{0.1}\text{MnO}_3/\text{SrNb}_{0.01}\text{Ti}_{0.99}\text{O}_3$) interfaces exhibited a colossal positive magnetoresistance under low magnetic fields (13). As another example shown in Figure 3B, good ferroelectricity of our bismuth ferrite (BiFeO_3) films was confirmed by local measurements using a piezoresponse force microscope (14, 15). A switchable diode effect, diode direction reversible by switching fer-

roelectric polarization, was observed in the BiFeO_3 ferroelectric thin films, in which the polarization-modulated interfacial barrier played an important role (14, 15). Furthermore, by using the migration of oxygen vacancies in strontium titanate (SrTiO_3) oxides (16), we proposed another strategy to produce the switchable diode and photovoltaic effect without using ferroelectric materials. The results are shown in Figure 3C. We revealed that the band bending induced by the motion of oxygen vacancies is the driving force for the switch between the two states. Based on this strategy, one could design switchable photovoltaic devices.

In Figure 3D, an ultrafast photoelectric effect was observed in the $\text{La}_{0.7}\text{Sr}_{0.3}\text{MnO}_3/\text{Si}$ heterojunction (11, 12). When this junction was irradiated by a 1064-nm laser pulse of 25 ps duration, the rise time was ~ 210 ps, and the full width at half-maximum was ~ 650 ps for the photovoltaic pulse. An unusual lateral photovoltage induced by the Dember effect was discovered in this structure (17). Recently, much attention has been paid to perovskite oxides with wide bandgaps, because they are natural candidates for photoabsorption materials for next-generation ultraviolet (UV) photodetectors. We fabricated a solar-blind UV photodetector employing lanthanum aluminum oxide (LaAlO_3) perovskite oxide with a bandgap of 5.6 eV for the first time (18). The response showed a sharp cutoff at ~ 220 nm. The photocurrent response reached 71.8 mA/W at

200 nm (Figure 3E), and the quantum efficiency reached 44.6%, indicating a unique potential in deep-UV detection.

Terahertz spectroscopy

Since the invention of femtosecond titanium (Ti):Sapphire all-solid-state lasers in the early 1990s, coherent terahertz sources developed rapidly (19), and terahertz time-domain spectroscopy (THz-TDS) emerged as a powerful tool for exploring light-matter interactions. In 1994, group L04 built the first THz-TDS measurement system in mainland China, as illustrated in Figure 4A.

When photocarriers are excited at the interface of semiconductors, THz radiation can be generated through current transients, carrying important information such as carrier mobility, field evolution, and modulated material responses. For example, the gold/gallium arsenide (Au/GaAs) Schottky interface excited by a femtosecond laser

pulse results in fast Fermi-level bending due to carrier accumulation in the depletion layer. We revealed this mechanism by temperature-dependent pump-probe measurements with picosecond time resolution (20). As shown in Figure 4B, the radiation was produced from a bulk highly oriented pyrolytic graphite (HOPG) excited by femtosecond laser pulses at 800 nm. By varying the incident angle of the pumping laser and applying an external bias, it was confirmed that the photocarriers driven by the built-in field within the first few carbon atomic layers were responsible for the THz generation (21).

The THz vibrational modes in biomolecules are very sensitive to molecular configuration and conformation. We used THz-TDS measurements to investigate the absorption and dispersion of polycrystalline α - and γ -glycine in the spectral region of 0.5 THz–3.0 THz (22). On the other hand, biomolecular reactions in a physiological condition are very important in many biological and medical studies, but quite difficult to detect. After overcoming the issue of water absorption using our highly sensitive THz-TDS system, we successfully observed the molecular reactions in aqueous solutions of anticancer drug oxaliplatin with λ -DNA and M-DNA extracted from mouse liver. As shown in Figure 4C, the half-life of the reaction was about 4.0 h for λ -DNA and 12.9 h for M-DNA, which can be attributed to their differences in strand length, composition, and sequence of nucleic acids (23).

References

1. B. Y. Cheng *et al.*, *Acta Phys. Sin.* **3**, 861 (1994).
2. J. X. Fu, R. J. Liu, Z. Y. Li, *Appl. Phys. Lett.* **97**, 041112 (2010).
3. L. Lu, Z. Wang, arXiv:1611.01998.
4. L. Lu, J. D. Joannopoulos, M. Soljačić, *Nat. Phys.* **12**, 626–629 (2016).
5. Q. H. Yan *et al.*, *Nat. Phys.* (2016), www.nature.com/articles/s41567-017-0041-4.
6. S. Cao *et al.*, *Sci. Rep.* **5**, 8041 (2015).
7. S. Cao *et al.*, *Nano Res.* **9**, 306–316 (2016).
8. J. Tang, W. Geng, X. Xu, *Sci. Rep.* **5**, 9252 (2015).
9. Y. Sun *et al.*, *ACS Photonics* **4**, 369–377 (2017).
10. Y. Zhao *et al.*, *Opt. Express* **23**, 9211–9220 (2015).
11. K. J. Jin *et al.*, *Adv. Mater.* **21**, 4636–4640 (2009).
12. Y. Q. Feng *et al.*, *Sci. Rep.* **6**, 22382 (2016).
13. K. J. Jin *et al.*, *Phys. Rev. B* **71**, 184428 (2005).
14. A. Q. Jiang *et al.*, *Adv. Mater.* **23**, 1277–1281 (2011).
15. C. Wang *et al.*, *Appl. Phys. Lett.* **98**, 192901 (2011).
16. C. Ge *et al.*, *ACS Appl. Mater. Interfaces* **8**, 34590 (2016).
17. K. J. Jin *et al.*, *Appl. Phys. Lett.* **91**, 081906 (2007).
18. J. Xing *et al.*, *Opt. Lett.* **34**, 1675–1677 (2009).
19. L. Wang, in *Encyclopedia of Modern Optics*, vol. 5, G. Steel, B. D. Guenther, Eds. (Elsevier, New York, 2004), pp. 163–168.
20. Y. L. Shi *et al.*, *Appl. Phys. Lett.* **88**, 161109 (2006).
21. T. Ye *et al.*, *Sci. Rep.* **6**, 22798 (2016).
22. Y. L. Shi, L. Wang, *J. Phys. D* **38**, 3741–3745 (2005).
23. X. J. Wu *et al.*, *Appl. Phys. Lett.* **101**, 033704 (2012).

Ultrafast intense laser technology and physics

Yutong Li, Zhiyi Wei*,
Bingbing Wang, and Jie Zhang*

The pursuit of ultrashort laser pulses and ultraintense laser power has attracted interest from a wide range of disciplines since the creation of lasers. The invention of chirped pulse amplification (CPA) technology and the discovery of Kerr-lens mode locking (KLM) for the titanium (Ti) sapphire laser in 1985 and 1991, respectively, have enabled us to generate ultrahigh intensity laser pulses at tabletop scale. With remarkable progress in recent years, peak power up to several petawatts (PW) has been reported, and pulse durations of shorter than 50 attoseconds have been demonstrated, which not only provide unprecedented extreme conditions for exploring emerging physics and phenomena, but also open a new era for revealing the ultrafast dynamics of electrons. Since the National Research Institute of Physics, Academia Sinica, was founded in 1928, optics has been studied as one of the main disciplines, and considerable achievements in laser science and technology have been made in the past 90 years. Inheriting these developments and innovations in optical physics, the Institute of Physics (IOP), Chinese Academy of Sciences, has been working toward ultrafast lasers and intense laser-matter interactions since 1997. Until now, only carrier-envelope phase (CEP)-controlled few-cycle lasers have been capable of realizing low-noise frequency comb generation and attosecond laser pulses; however, intense laser power—up to 1.16 PW—has now been generated from the in-house Ti-sapphire laser facility [XL-III (eXtreme Light)]. These laser systems have provided an experimental platform for research on laser-driven particle acceleration, novel laser-driven X-ray and THz radiation sources, laboratory astrophysics, fundamental physical processes relevant to advanced nuclear fusion concepts, long-distance propagation of femtosecond (fs) laser pulses in air (1, 2), and ultrarelativistic laser-matter interactions. Below, we briefly review some previously published results.

CEP control of few-cycle femtosecond lasers

It has been challenging work generating the shortest laser pulse. By using chirped mirrors to compensate for dispersion, we have generated 6-fs pulses from an in-house Ti-sapphire laser oscillator (3). An ultrabroad saddle-shaped spectrum was designed to enable superior results in CEP measurements, based on the difference fre-